

Hard-sphere solids near close packing: Testing theories for crystallization

Benito Groh and Bela Mulder

FOM Institute for Atomic and Molecular Physics, Kruislaan 407, 1098 SJ Amsterdam, The Netherlands

(Received 8 July 1999)

The freezing transition of hard spheres has been well described by various versions of density-functional theory (DFT). These theories should possess the close-packed crystal as a special limit, which represents an extreme testing ground for the quality of such liquid-state based theories. We therefore study the predictions of DFT for the structure and thermodynamics of the hard-sphere crystal in this limit. We examine the Ramakrishnan-Yussouff (RY) approximation and two variants of the fundamental-measure theory (FMT) developed by Rosenfeld and co-workers. We allow for general shapes of the density peaks, going beyond the common Gaussian approximation. In all cases we find that upon approaching close packing, the peak width vanishes proportionally to the free distance a between the particles and the free energy depends logarithmically on a . However, different peak shapes and next-to-leading contributions to the free energy result from the different approximate functionals. For the RY theory, within the Gaussian approximation, we establish that the crystalline solutions form a closed loop with a stable and an unstable branch both connected to the close-packing point at $a=0$, consistent with the absence of a liquid-solid spinodal. That version of FMT that has previously been applied to freezing, predicts asymptotically steplike density profiles confined to the cells of self-consistent cell theory. But a recently suggested improved version which employs tensor weighted densities yields wider and almost Gaussian peaks that are shown to be in very good agreement with computer simulations.

PACS number(s): 61.20.Gy, 64.70.Dv, 61.50.Ah, 64.10.+h

I. INTRODUCTION

Some twenty years ago Alexander and McTague applied the formalism of Landau theory to the freezing transition of atomic materials [1]. Using symmetry arguments they suggested that a bcc crystal should be the universally favored crystal structure, independent of interaction details. This theory attempts to describe the solid as a small, spatially periodic perturbation of a liquid. In a recent paper [2] we argued that such an approach should only be valid near the liquid-solid spinodal, at which the liquid state becomes locally unstable. The position of the spinodal is determined by the Fourier transform of the liquid direct correlation function \tilde{c} , and is given by the smallest density ρ for which the equation

$$\rho \tilde{c}(\rho, k) = 1 \quad (1)$$

has a solution. Moreover, the perturbative approach does not apply to the local minima of the free energy in order-parameter space, which correspond to metastable or stable crystals, but rather to its saddle points. For the latter we confirmed universal behavior near the spinodal, which may have implications for nucleation [2].

The hard-sphere fluid has become the canonical model for freezing, since it captures in the most simple form the dominant packing effects while attractive interactions are believed to play only a secondary role. The best current theories for hard-sphere freezing are various versions of density-functional theory (DFT) [3–7]. Usually they are explicitly constructed to reproduce the Percus-Yevick approximation c_{PY} for the hard-sphere direct correlation function. In Fig. 1 we show the values of $\tilde{c}_{PY}(\rho, k)$ evaluated at the wave number $k_{\max}(\rho)$ corresponding to the maximum at a given den-

sity ρ . One finds that there is no solution to Eq. (1) at physical densities ρ below the space filling density $6/\pi\sigma^{-3}$ where σ is the particle diameter (at and beyond this limit c_{PY} is not defined). This implies that those DFTs do not exhibit a liquid-solid spinodal at all. Therefore the saddle point solution branch of the stationarity equation derived from the density functional cannot connect to the liquid branch when the bulk density is increased. On the other hand, hard-core systems are characterized by a close-packing density as the maximum possible density of a given crystal structure. Upon approaching this limit a suitably defined crystalline order parameter, e.g., the inverse width of the density peaks, will diverge along the stable (minimum) branch. One may surmise that that is also true along the saddle point branch. Thus an alternative scenario to the bifurcation of a crystalline solution from the liquid at a spinodal point as discussed in Ref. [2], are two solid solution branches smoothly connected to each other at low densities which diverge at close packing and are completely isolated from the liquid. In order to test this hypothesis in the present work we examine the close-packing limit in detail using DFTs that have previously been applied to the low-density solid near the phase transition.

Clearly, the strong localization of the particles in this limit provides an extreme case for such liquid-state based theories. Hence it is a good testing ground for assessing the qualities of different approximations. In contrast to most DFT studies of the hard-sphere solid we do not restrict the shape of the density peaks to Gaussians, but allow for general spherically symmetric peaks. This is especially interesting for the completely anharmonic hard-sphere crystal for which there is no a priori argument to justify Gaussians, even for small amplitude particle oscillations.

The starting point of density-functional theory is the free energy functional of the inhomogeneous particle density $\rho(\mathbf{r})$ with the general form

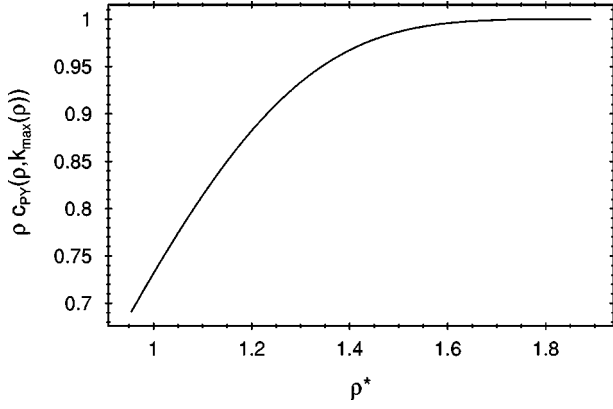


FIG. 1. The left-hand side of Eq. (1) for the hard-sphere direct correlation function in the Percus-Yevick approximation. The wave number $k_{\max}(\rho)$ corresponds to the maximum of $c_{\text{PY}}(\rho, k)$ at a given density $\rho = \rho^* \sigma^{-3}$. The curve lies below unity for all admissible densities $\rho^* < 6/\pi = 1.910$, i.e., for packing fractions $\eta = \rho^* \pi/6 < 1$, which means that there is no liquid-solid spinodal. The close-packing limit occurs at $\rho^* = \sqrt{2}$.

$$F[\rho(\mathbf{r})] = F_{\text{id}}[\rho(\mathbf{r})] + F_{\text{ex}}[\rho(\mathbf{r})]. \quad (2)$$

The ideal gas contribution is given by [$\beta = 1/(k_B T)$]

$$\beta F_{\text{id}}[\rho(\mathbf{r})] = \int d^3 r \rho(\mathbf{r}) [\ln \rho(\mathbf{r}) \lambda^3 - 1] \quad (3)$$

with the thermal de Broglie wavelength λ . While the excess part F_{ex} is not known exactly, a large number of approximate forms have been suggested and applied to various problems in the last decades [3–7]. As we do not strive for completeness we will consider only two representative variants in this paper: the Ramakrishnan-Yussouff functional [8,9] which is one of the first and simplest approximations that have been studied, and the fundamental measure functional developed by Rosenfeld and co-workers [10,11] which at the present is believed to provide the best theoretical description of the hard-sphere fluid. From a given functional the equilibrium density distribution at a given bulk density ρ_b is obtained by minimization under the constraint $V^{-1} \int d^3 r \rho(\mathbf{r}) = \rho_b$. The value of the functional at its minimum is the actual free energy of the system. For both functionals we performed numerical calculations at a series of bulk densities as well as an analytical analysis of the close-packing limit which enables us to determine the asymptotic density profile and free energy.

II. RAMAKRISHNAN-YUSSOUFF THEORY

A. Density functional and equilibrium profiles

The Ramakrishnan-Yussouff functional follows from a density expansion of F_{ex} around the homogeneous state truncated at the quadratic term:

$$\begin{aligned} \beta F_{\text{ex}}/V = & \beta f_{\text{ex}}(\rho_b) - \frac{1}{2V} \int d^3 r d^3 r' [\rho(\mathbf{r}) - \rho_b] \\ & \times [\rho(\mathbf{r}') - \rho_b] c(\bar{\rho}, |\mathbf{r} - \mathbf{r}'|). \end{aligned} \quad (4)$$

Here f_{ex} is the free energy density and c the direct correlation function (DCF) of the hard-sphere liquid at an effective density $\bar{\rho}$, both of which are commonly approximated by the analytically known solutions of the Percus-Yevick integral equation. In a solid the density consists of a sum of identical peaks centered at the lattice sites \mathbf{R} :

$$\rho(\mathbf{r}) = \sum_{\mathbf{R}} \rho_{\Delta}(\mathbf{r} - \mathbf{R}). \quad (5)$$

Throughout this paper it is assumed that the peaks are normalized

$$\int d^3 r \rho_{\Delta}(\mathbf{r}) = 1 \quad (6)$$

and that the nearest-neighbor distance R_{NN} in the lattice is determined by the bulk density, $R_{\text{NN}}/\sigma = (\rho_{\text{CP}}/\rho_b)^{1/3}$ where σ is the particle diameter and ρ_{CP} is the maximum possible density. In order to reduce the dimensionality of the integrations we moreover assume that ρ_{Δ} is spherically symmetric. Deviations from this symmetry exist [12,13], but are small especially near close packing [14]. However, in contrast to most solid phase calculations which assume ρ_{Δ} to be Gaussian here we do not restrict its shape.

By insertion of Eq. (5) in Eq. (4) one obtains

$$\begin{aligned} \beta F_{\text{ex}}/V = & \beta f_{\text{ex}}(\rho_b) \\ & + \frac{1}{2} \rho_b^2 \tilde{c}(\bar{\rho}, k=0) - \frac{1}{2} \rho_b \\ & \times \sum_{\mathbf{R}} \int d r r^2 \int d r' r'^2 \rho_{\Delta}(r) \rho_{\Delta}(r') w(r, r', R), \end{aligned} \quad (7)$$

where \tilde{c} is the Fourier transformed DCF and the integral kernel is given by

$$\begin{aligned} w(r, r', R) = & 2\pi \int_0^{2\pi} d\phi_{12} \int_{-1}^1 d\cos\theta \int_{-1}^1 d\cos\theta' \\ & \times c[\bar{\rho}, (r^2 + r'^2 + R^2 + 2rR\cos\theta \\ & - 2r'R\cos\theta' - 2rr'\cos\gamma)^{1/2}]. \end{aligned} \quad (8)$$

The angles θ , θ' , and γ are those between \mathbf{r} and \mathbf{R} , \mathbf{r}' and \mathbf{R} , and \mathbf{r} and \mathbf{r}' , respectively, and $\cos\gamma = \cos\theta\cos\theta' + \cos\phi_{12}\sin\theta\sin\theta'$. The contribution from $R=0$ simplifies to

$$w(r, r', 0) = \frac{8\pi^2}{rr'} \int_{|r-r'|}^{r+r'} d r_{12} r_{12} c(\bar{\rho}, r_{12}). \quad (9)$$

Without loss of generality one may restrict the domain of ρ_{Δ} to the Wigner-Seitz cell, so that the ideal contribution to the functional can be written as

$$\beta F_{\text{id}}/V = 4\pi\rho_b \int d r r^2 \rho_{\Delta}(r) [\ln \rho_{\Delta}(r) \lambda^3 - 1]. \quad (10)$$

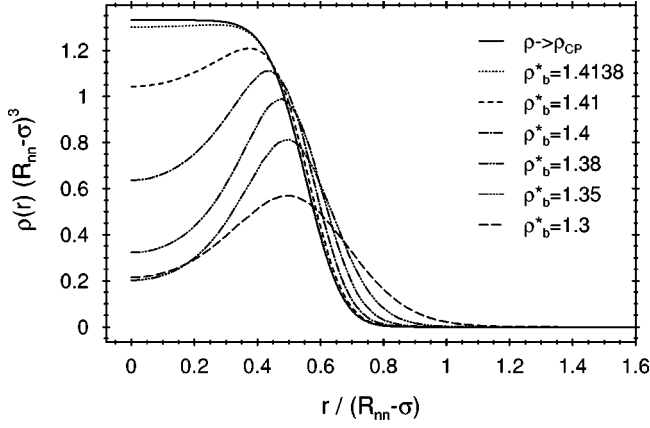


FIG. 2. Density profiles in a high density fcc crystal calculated from Ramakrishnan-Yussouff DFT. Note that the distance r from the lattice site and the density are scaled by the free distance $a = R_{NN} - \sigma$, which varies over 2.5 orders of magnitude in this density range.

By minimizing and taking into account the normalization Eq. (6) one finds the stationarity equation

$$\rho_{\Delta}(r) = \frac{\exp\left[(1/4\pi) \sum_{\mathbf{R}} \int dr' r'^2 \rho_{\Delta}(r') w(r, r', R)\right]}{4\pi \int dr r^2 \exp\left[(1/4\pi) \sum_{\mathbf{R}} \int dr' r'^2 \rho_{\Delta}(r') w(r, r', R)\right]}. \quad (11)$$

The Percus-Yevick approximation for the hard-sphere DCF has the simple form

$$c(\bar{\rho}, r) = [c_0(\bar{\rho}) + c_1(\bar{\rho})r + c_3(\bar{\rho})r^3] \Theta(\sigma - r). \quad (12)$$

The density dependence of the coefficients c_i can for example be found in Ref. [15]. In the present context its most important feature is the cutoff at the particle diameter which leads to $w(r, r', R) = 0$ for $R - r - r' > \sigma$. Hence for the strongly peaked profiles in high density solids only the first shell of lattice vectors ($|\mathbf{R}| = R_{NN}$) and the term with $R = 0$ must be taken into account. We have calculated $w(r, r', R_{NN})$ by numerical integration using the trapezoidal rule with 50^3 mesh points, while an analytical expression for $w(r, r', 0)$ was derived from Eq. (9). The stationarity equation is then discretized in r and solved by iteration. An underrelaxation scheme

$$\rho^{(n+1)} = \omega \rho_{\text{new}}^{(n)} + (1 - \omega) \rho^{(n)} \quad (13)$$

proved helpful to ensure convergence. Here $\rho^{(n)}$ is the profile after the n th iteration and $\rho_{\text{new}}^{(n)}$ is the right hand side of Eq. (11) calculated from $\rho^{(n)}$. A typical value of the constant ω was 0.2.

The resulting profiles are shown in Fig. 2. Their width scales with the free distance $a = R_{NN} - \sigma$ that a sphere can move into the direction to its neighbor if the latter is kept fixed. The profile shapes approach a limiting form discussed below. Their most striking property is the occurrence of a

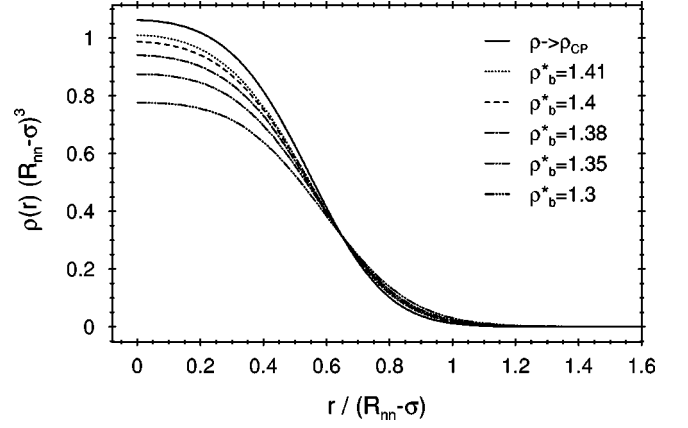


FIG. 3. The same as Fig. 2 but using $\bar{\rho} = 0.95$ as the density argument of the DCF. In this case the profiles are monotonic.

maximum at intermediate distances r . This unphysical behavior vanishes in the close-packing limit. The DCF has been evaluated at the bulk density $\bar{\rho} = \rho_b$. This most obvious choice has the disadvantage that the solid has a higher free energy than the liquid at all densities, as already pointed out in Ref. [16]. In the earliest DFT work the density of the coexisting liquid has been used instead, but that is not very reasonable when high density solids are considered. Other schemes to select a density $\bar{\rho}$ of an “effective liquid” have been proposed Ref. [16,17,4], which always imply $\bar{\rho} < \rho_b$. Figure 3 shows density profiles obtained with an arbitrarily chosen value $\bar{\rho}^* = \bar{\rho}\sigma^3 = 0.95$ which is close to the freezing density. Now the maximum does not occur and the convergence to the limiting shape is faster. The profiles are considerably flatter at small r than a Gaussian of the same width.

B. Close-packing limit

The results shown in Figs. 2 and 3 clearly demonstrate that, in spite of contrary claims [18,19], simple density-functional theories based on the Percus-Yevick DCF do exhibit a well-defined close-packing limit at which the peak width goes to zero. We will analyze this limit in more detail in the following. Let us assume that for small $a = R_{NN} - \sigma$ the profile behaves as

$$\rho_{\Delta}(r) = \frac{1}{\Delta^3} \rho_0\left(\frac{r}{\Delta}\right) \quad (14)$$

with a width $\Delta = a/\alpha$ where $\Delta, a \rightarrow 0$ with α fixed. We shall show that the stationarity equation has a solution consistent with these assumptions. The ideal free energy in this limit becomes (with $N = \rho_b V$ and $s = r/\Delta$)

$$\beta F_{\text{id}}/N = 4\pi \int_0^{\infty} ds s^2 \rho_0(s) [\ln \rho_0(s) - 3 \ln(\Delta/\lambda) - 1]. \quad (15)$$

The relevant contributions to F_{ex} are

$$w(r = s\Delta, r' = s'\Delta, 0) = 16\pi^2 c(\bar{\rho}, 0) + O(\Delta) \quad (16)$$

and

$$\begin{aligned}
w(r=s\Delta, r'=s'\Delta, R_{\text{NN}}) &= 2\pi \int_0^{2\pi} d\phi_{12} \int_{-1}^1 dx \int_{-1}^1 dx' \\
&\quad \times c(\bar{\rho}, \sigma [1 + \Delta/\sigma(\alpha + sx - s'x') + O(\Delta^2)]) \\
&= 4\pi^2 c(\bar{\rho}, \sigma) \tilde{w}(s, s', \alpha) + O(\Delta), \tag{17}
\end{aligned}$$

where

$$\begin{aligned}
\tilde{w}(s, s', \alpha) &= \frac{1}{ss'} \int_{-s}^s ds_3 \int_{-s'}^{s'} ds_3' \Theta(s_3' - s_3 - \alpha) \\
&= \begin{cases} 0, & s' + s < \alpha, \\ (s + s' - \alpha)^2 / (2ss'), & s' + s > \alpha, \quad -\alpha < s' - s < \alpha, \\ 2(1 - \alpha/s'), & s' - s > \alpha, \\ 2(1 - \alpha/s), & s' - s < -\alpha. \end{cases} \tag{18}
\end{aligned}$$

Thus we finally have in leading order in Δ

$$\begin{aligned}
\beta F_{\text{ex}}/N &= -2\pi^2 N_{\text{NN}} c(\bar{\rho}, \sigma) \\
&\quad \times \int_0^\infty ds s^2 \int_0^\infty ds' s'^2 \rho_0(s) \rho_0(s') \tilde{w}(s, s', \alpha) \\
&\quad + \text{const} = \Phi + \text{const}, \tag{19}
\end{aligned}$$

where N_{NN} denotes the number of nearest neighbors.

The total free energy can now be minimized in two different ways. First, one can restrict to profiles of a fixed shape $\rho_0(s)$, e.g., Gaussians, and differentiate only with respect to the scaled width α for fixed a which gives

$$3 = -\alpha \frac{\partial \Phi}{\partial \alpha}. \tag{20}$$

Due to the form of $w(s, s', \alpha)$ for $\alpha \rightarrow \infty$ one has $\Phi \rightarrow 0$ and thus the right hand side of Eq. (20) also decays. On the other hand, for $\alpha \rightarrow 0$ Φ tends to a positive constant [since $c(\bar{\rho}, \sigma)$ is negative], thus its derivative will be negative for sufficiently well behaved $\rho_0(s)$. Therefore, the right hand side of Eq. (20) is zero both at $\alpha=0$ and $\alpha=\infty$ and positive in between which implies a maximum at a finite value of α . This can be explicitly checked for Gaussians [$\rho_0(s) = \pi^{-3/2} \exp(-s^2)$] and step functions [$\rho_0(s) = 3/(4\pi) \Theta(1-s)$] for which the integrals in Eq. (19) yield $\frac{1}{2}[1 - \text{erf}(\alpha/\sqrt{2})]$ and $\frac{1}{2} - \frac{3}{5}\alpha + \frac{1}{4}\alpha^3 - \frac{3}{32}\alpha^4 + \frac{1}{320}\alpha^5$. Depending on the height of this maximum Eq. (20) has zero or two solutions. In the first case there are no stationary points with vanishing peak width at $\rho_b = \rho_{cp}$. This is the case for the ‘‘Onsager solid’’ discussed in Ref. [2] which belongs to the same class of approximate functionals, but with $c(\bar{\rho}, r)$ replaced by its low-density limit $-\Theta(\sigma - r)$. If $-c(\bar{\rho}, \sigma)$ is larger [e.g., $c_{\text{PY}}(\rho_{cp}^{\text{fcc}}, \sigma) = -20.345$] the solution with smaller α corresponds to a saddle point and the solution with larger α to the stable solid minimum. We emphasize that the widths $\Delta = a/\alpha$ for both solutions tend to zero for $\rho_b \rightarrow \rho_{cp}$. In Fig. 4 we display the results obtained for fcc and bcc solids, employing Gaussian profiles and $\bar{\rho} = \rho_b$ (fcc: $\rho_{cp}^* = \sqrt{2}$, $N_{\text{NN}} = 12$; bcc: $\rho_{cp}^* = 3\sqrt{3}/4$, $N_{\text{NN}} = 8$). We also include numerical solutions of $\partial F/\partial \Delta = 0$ for the nonasymptotic functional discussed above, evaluated for Gaussians. They approach the asymptotics quite slowly, especially for the saddle points. At low densities both branches are connected at an inflection point below which no solidlike solutions exist.

Alternatively one can differentiate the asymptotic functional in Eqs. (15) and (19) with respect to the profile $\rho_0(s)$. Here one may set $\alpha = 1$ without loss of generality. This leads to the Euler Lagrange equation

$$\rho_0(s) = \frac{\exp\left[\pi N_{\text{NN}} c(\bar{\rho}, \sigma) \int_0^\infty ds' s'^2 \rho_0(s') \tilde{w}(s, s', 1)\right]}{4\pi \int_0^\infty ds s^2 \exp\left[\pi N_{\text{NN}} c(\bar{\rho}, \sigma) \int_0^\infty ds' s'^2 \rho_0(s') \tilde{w}(s, s', 1)\right]}. \tag{21}$$

Its solutions, which represent the asymptotic profile *shape*, obviously only depend on the value of c at $r = \sigma$, because near close packing the distance between two interacting particles is always very close to σ . The resulting shapes, shown in Figs. 2 and 3, are rather flat close to the lattice site and decay strongly around $r/a = 0.6$, so they are definitely non-Gaussian.

The iteration never converged to a second solution that would represent the saddle point, even when started from the Gaussian saddle point discussed above. It has been conjectured in a DFT study of the isotropic-nematic transition of

hard rods [20] that in general the saddle point is not accessible by iteration because it corresponds to an unstable fixed point (see also Ref. [21]).

We mention a subtle point in connection with Eq. (21). Due to the form of \tilde{w} the right hand side goes to a constant for $s \gg 1$, which means that no normalized solution on $[0, \infty)$ can exist. However, as mentioned above, one may restrict to functions with a finite support [e.g., $r < R_{\text{NN}}/2$, i.e., $s < R_{\text{NN}}/(2a)$]. For the numerical program indeed a much lower cutoff was used. In principle the solution now depends

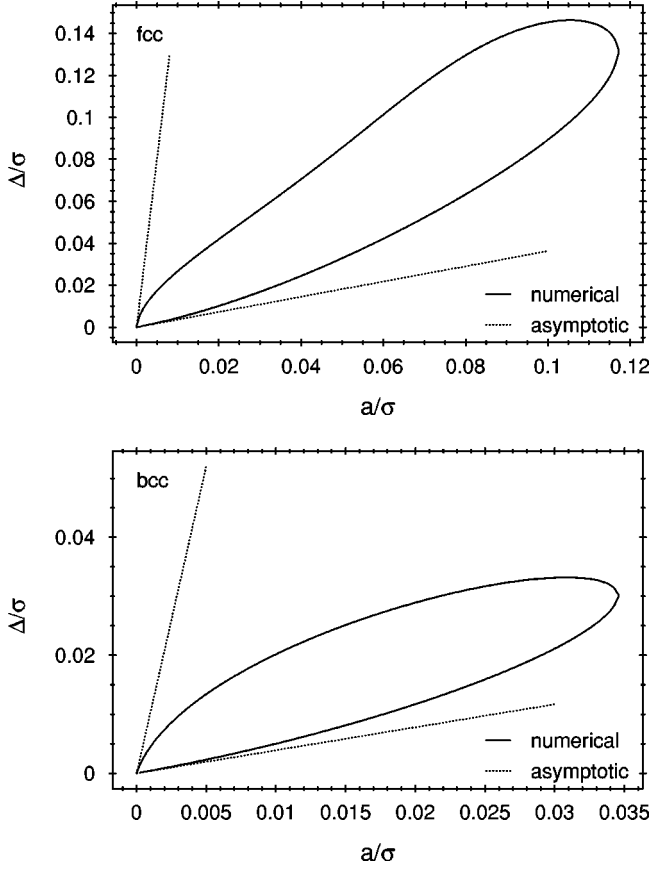


FIG. 4. Widths Δ corresponding to minima (lower branches) and saddle points (upper branches) of the Ramakrishnan-Yussouf functional restricted to Gaussian profiles for fcc and bcc solids. The asymptotic linear behavior indicated by the dashed lines was calculated from Eq. (20).

on the cutoff, but in practice this dependence is extremely weak because the constant approached for large s is of the order of $\exp[\frac{1}{2}N_{\text{NNC}}(\bar{\rho}, \sigma)] \approx 10^{-53}$ so that the contributions from the tail of $\rho_0(s)$ are negligible for any reasonable value of the cutoff. Similar remarks apply to Eq. (11).

The free energy of the solid is determined by inserting the calculated equilibrium profiles into the density functional. Its asymptotic behavior is given by

$$\beta F/N = -3 \ln a + f_0 + O(a). \quad (22)$$

The leading logarithmic contribution stems from F_{id} and is in accordance with the result of free volume theory [22] and cell theory [23,24]. It has been proven exact for parallel hard cubes [25] and for finite hard-sphere systems [26] and is generally believed to be exact also in the thermodynamic limit. The various theories differ in their prediction for the constant f_0 . In the Ramakrishnan-Yussouf approach (with $\bar{\rho} = \rho_b$) for an fcc solid we obtain $f_0 = 21.7$ which is far above the molecular dynamics result $f_0 = -1.493$ [27]. As shown in Fig. 5 the asymptotic form is approached quite slowly, i.e., the higher order terms in Eq. (22) are important up to high densities (which probably will also produce a bad equation of state). The free energies from the full minimization are only slightly below those for the best Gaussian profile (Fig. 5).

III. FUNDAMENTAL-MEASURE THEORY

A. Density functional

Fundamental measure theory at present represents the best available DFT for strongly inhomogeneous hard-sphere fluids. In contrast to most previous approaches it does not depend on the direct correlation function as an input, but rather reproduces the Percus-Yevick correlation function as an output of the theory in the homogeneous limit. While the original expressions [10] gave a divergent excess free energy for strongly localized particles, a recent empirical modification proved suitable also for the description of the freezing transition [11]. We will call this version FMT1. Another new approximation has recently been suggested by Tarazona and Rosenfeld [28] based on more fundamental grounds. They presented a new derivation of FMT by enforcing the functional to reduce to exactly known expressions in the zero- and one-dimensional limit. They obtained a more complicated expression for one of the excess free energy contributions that cannot be expressed in terms of weighted densities and also does not reduce to the Percus-Yevick free energy in the homogeneous limit. They also suggested a simplification by rescaling a certain expansion of this exact expression, which we adopt as FMT2. Due to its construction we expect FMT2 to provide a better description of the high-density crystal in which the individual particles are confined to quasi-zero-dimensional cages formed by their neighbors.

For a one-component hard-sphere fluid in three dimensions the fundamental-measure functional has the form

$$\beta F_{\text{ex}}[\rho(\mathbf{r})] = \int d^3r \sum_{i=1}^3 \phi_i[n_\alpha(\mathbf{r})], \quad (23)$$

where the functions ϕ_i depend only on the weighted densities

$$n_\alpha(\mathbf{r}) = \int d^3r' \rho(\mathbf{r}') w_\alpha(\mathbf{r} - \mathbf{r}'). \quad (24)$$

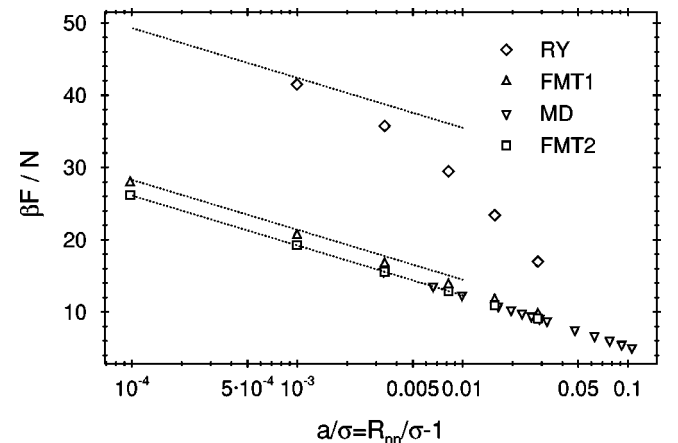


FIG. 5. Free energies per particle of high density solids from the Ramakrishnan-Yussouf DFT, the two versions of fundamental-measure DFT, and from molecular dynamics [27]. The de Broglie wave length has been set to the particle diameter. The asymptotic behavior indicated by the dotted lines is logarithmic in the free distance a [see Eq. (22)] in all cases.

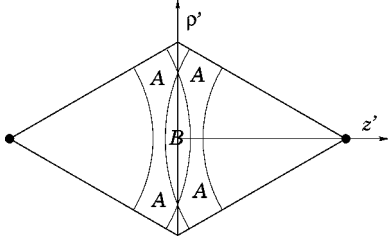


FIG. 6. The space between two nearest-neighbor sites (black dots) in a crystal. The radii of the spheres are $\sigma/2 \pm O(\Delta)$ where Δ is the width of the (spherical) density peaks. The weighted densities in region A are only influenced from one site while in B both sites contribute. In the remaining space the excess free energy densities ϕ_i are negligible.

In FMT1 only one vectorial and two independent scalar weight functions occur:

$$\begin{aligned} w_3(r) &= \Theta\left(\frac{\sigma}{2} - r\right), \\ w_2(r) &= \delta\left(\frac{\sigma}{2} - r\right), \\ \mathbf{w}_{V2}(\mathbf{r}) &= \frac{\mathbf{r}}{r} \delta\left(\frac{\sigma}{2} - r\right). \end{aligned} \quad (25)$$

For FMT2 a tensor weight function is necessary:

$$\hat{\mathbf{w}}_{ij}(\mathbf{r}) = \frac{r_i r_j}{r^2} \delta\left(\frac{\sigma}{2} - r\right). \quad (26)$$

The expressions for the excess free energy density are

$$\phi_1 = -\frac{n_2}{\pi\sigma^2} \ln(1 - n_3), \quad (27)$$

$$\phi_2 = \frac{n_2^2 - n_{V2}^2}{2\pi\sigma(1 - n_3)}, \quad (28)$$

$$\phi_3^{\text{FMT1}} = \frac{(n_2^2 - n_{V2}^2)^3}{24\pi n_2^3 (1 - n_3)^2}, \quad (29)$$

$$\phi_3^{\text{FMT2}} = \frac{9}{8\pi} \frac{\det \hat{\mathbf{n}}}{(1 - n_3)^2}. \quad (30)$$

The density ansatz Eq. (5) induces a corresponding form for the weighted densities

$$n_\alpha(\mathbf{r}) = \sum_{\mathbf{R}} n_\Delta^{(\alpha)}(\mathbf{r} - \mathbf{R}) \quad (31)$$

with

$$n_\Delta^{(\alpha)}(\mathbf{r}) = \int d^3 r' \rho_\Delta(\mathbf{r}') w_\alpha(\mathbf{r} - \mathbf{r}'). \quad (32)$$

If ρ_Δ is spherically symmetric the calculation of the weighted densities reduces to one-dimensional integrations

$$\begin{aligned} n_\Delta^{(3)}(r) &= \frac{\pi}{r} \int_{|r-\sigma/2|}^{r+\sigma/2} dr' r' \left(\frac{\sigma^2}{4} - (r-r')^2 \right) \rho_\Delta(r') \\ &+ \Theta\left(\frac{\sigma}{2} - r\right) 4\pi \int_0^{\sigma/2-r} dr' r'^2 \rho_\Delta(r'), \end{aligned} \quad (33)$$

$$n_\Delta^{(2)}(r) = \frac{\pi\sigma}{r} \int_{|r-\sigma/2|}^{r+\sigma/2} dr' r' \rho_\Delta(r'), \quad (34)$$

$$\mathbf{n}_\Delta^{(V2)}(\mathbf{r}) = \frac{\mathbf{r}}{r} \frac{\pi}{r^2} \int_{|r-\sigma/2|}^{r+\sigma/2} dr' r' \left(r^2 - r'^2 + \frac{\sigma^2}{4} \right) \rho_\Delta(r'). \quad (35)$$

In this case the matrix $\hat{\mathbf{n}}_\Delta(\mathbf{r})$ [defined by $\hat{\mathbf{n}}(\mathbf{r}) = \sum_{\mathbf{R}} \hat{\mathbf{n}}_\Delta(\mathbf{r} - \mathbf{R})$] is diagonal in any coordinate system aligned with \mathbf{r} . An explicit calculation yields the eigenvalues

$$\begin{aligned} n_\Delta^{(11)}(r) &= n_\Delta^{(22)}(r) = \frac{\pi}{2r_\sigma^3} \int_{|\sigma/2-r|}^{r+\sigma/2} dr' r' \\ &\times \left[4r^2 r'^2 - \left(\frac{\sigma^2}{4} - r'^2 - r^2 \right)^2 \right] \rho_\Delta(r') \end{aligned} \quad (36)$$

and

$$n_\Delta^{(33)}(r) = \frac{\pi}{r_\sigma^3} \int_{|\sigma/2-r|}^{r+\sigma/2} dr' r' \left(\frac{\sigma^2}{4} - r'^2 + r^2 \right)^2 \rho_\Delta(r'). \quad (37)$$

Note that $\text{Tr} \hat{\mathbf{n}}_\Delta(\mathbf{r}) = n_\Delta^{(2)}(r)$. As ρ_Δ is a strongly peaked function of width Δ the weighted densities $n_\Delta^{(2)}(\mathbf{r})$, $\mathbf{n}_\Delta^{(V2)}(\mathbf{r})$, and $\hat{\mathbf{n}}_\Delta(\mathbf{r})$ have appreciable values only for $|r - \sigma/2| \leq \Delta$ while $n_\Delta^{(3)}(r)$ tends to 1 for much smaller r and to 0 for much larger r . Thus for small Δ at any point \mathbf{r} in a solid at most two terms contribute appreciably to the sum in Eq. (31).

We only consider fcc solids. By exploiting the crystal symmetry the integration in Eq. (23) can be restricted to a simplex corresponding to 1/48 of the unit cell. In a coordinate system aligned with the conventional cubic unit cell its vertices are

$$\begin{aligned} (0,0,0), \quad R_{\text{NN}} \left(\frac{1}{\sqrt{2}}, 0, 0 \right), \\ R_{\text{NN}} \left(\frac{1}{2\sqrt{2}}, \frac{1}{2\sqrt{2}}, 0 \right), \quad R_{\text{NN}} \left(\frac{1}{2\sqrt{2}}, \frac{1}{2\sqrt{2}}, \frac{1}{2\sqrt{2}} \right). \end{aligned} \quad (38)$$

It will be helpful to distinguish between the region A, that is ‘‘affected’’ by only one lattice site, and the region B affected by two sites, i.e., the set of those points whose distance to two sites differs from $\sigma/2$ by a length of order Δ . As depicted in Fig. 6 region B consists of lens shaped sets around the midpoints between neighboring sites. Here the integrands $\phi_i[n_\alpha(\mathbf{r})]$ do not depend on the azimuthal angle around the line joining the sites, thus only a two-dimensional numerical integration over cylindrical coordinates ρ' and z' must be performed. In order to compute the full $\hat{\mathbf{n}}$ in region B the

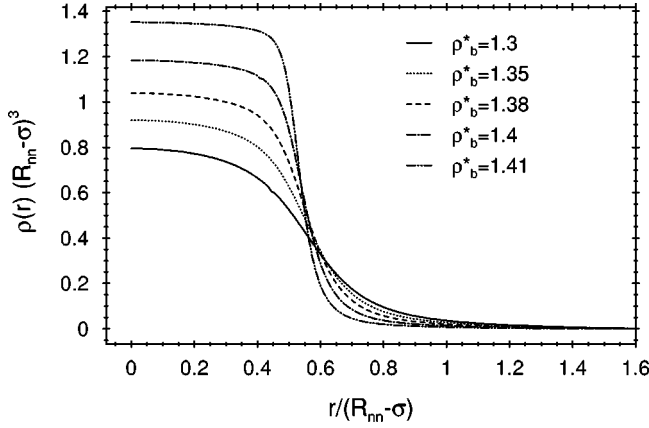


FIG. 7. Density profiles obtained from the fundamental-measure theory FMT1.

contribution from one of the sites must be transformed to the coordinate system determined by the direction to the other site. This is accomplished by a rotation around an axis perpendicular to this direction by the angle γ given by

$$\begin{aligned} \cos \gamma &= \frac{\mathbf{r}_+ \cdot \mathbf{r}_-}{r_+ r_-} \\ &= \frac{\rho'^2 + z'^2 - R_{\text{NN}}^2/4}{\{[\rho'^2 + (z' + R_{\text{NN}}/2)^2][\rho'^2 + (z' - R_{\text{NN}}/2)^2]\}^{1/2}}. \end{aligned} \quad (39)$$

Since in region A $n_\alpha(\mathbf{r})$ depends only on the distance to the nearest lattice site the corresponding integration can even be reduced to one dimension after the angular factors stemming from the shape of the simplex have been worked out analytically. In practice a sufficiently large cutoff Δ (typically $\Delta \approx 2a$) was chosen beyond which $\rho_\Delta(r)$ is assumed to be zero, and the integrals over A and B were calculated separately. This approach proved to be much faster and more accurate than a straightforward 2d integration over the whole simplex, because then the integrand is essentially zero in large parts of the integration region.

B. Equilibrium profiles

In order to determine the equilibrium density profile under the constraint of spherical symmetry the functional derivatives of F_{ex} are calculated. We first write

$$\frac{\delta \beta F_{\text{ex}}}{\delta \rho_\Delta(r)} = \int d^3 r' \sum_{i,\alpha} \frac{\partial \phi_i}{\partial n_\alpha} \frac{\delta n_\alpha(\mathbf{r}')}{\delta \rho_\Delta(r)} \quad (40)$$

and

$$\frac{\delta n_\alpha(\mathbf{r}')}{\delta \rho_\Delta(r)} = \frac{\delta}{\delta \rho_\Delta(r)} \sum_{\mathbf{R}} n_\Delta^{(\alpha)}(\mathbf{r}' - \mathbf{R}) = \sum_{\mathbf{R}} \left. \frac{\delta n_\Delta^{(\alpha)}(\mathbf{d})}{\delta \rho_\Delta(r)} \right|_{\mathbf{d}=\mathbf{r}'-\mathbf{R}}. \quad (41)$$

For $n_\Delta^{(3)}(d)$ the second term in Eq. (33) is rewritten as $\Theta(\sigma/2 - d)[1 - \int_{\sigma/2-d}^{\infty} dr' r'^2 \rho_\Delta(r')]$ which leads to

$$\begin{aligned} \frac{\delta n_\Delta^{(3)}}{\delta \rho_\Delta(r)} &= \left[\frac{\pi r}{d} \left(\frac{\sigma^2}{4} - (r-d)^2 \right) \right. \\ &\quad \left. - 4\pi r^2 \Theta\left(\frac{\sigma}{2} - d\right) \right] \Theta\left(\left|d - \frac{\sigma}{2}\right| - r\right), \end{aligned} \quad (42)$$

where we assumed that always $r < \sigma/2 + d$. Furthermore one finds

$$\frac{\delta n_\Delta^{(2)}(d)}{\delta \rho_\Delta(r)} = \frac{\pi \sigma r}{d} \Theta\left(\left|d - \frac{\sigma}{2}\right| - r\right), \quad (43)$$

$$\frac{\delta \mathbf{n}_\Delta^{(V2)}(\mathbf{d})}{\delta \rho_\Delta(r)} = \mathbf{d} \frac{\pi r}{d^3} \left(d^2 - r^2 + \frac{\sigma^2}{4} \right) \Theta\left(\left|d - \frac{\sigma}{2}\right| - r\right). \quad (44)$$

For the tensor weighted density straightforward calculation leads to a similar but more lengthy expression. The partial derivatives $\partial \phi_i / \partial n_\alpha$ are easily obtained from Eqs. (27)–(29). The functional derivative can now be computed by inserting Eqs. (42)–(44) into Eq. (41) and that into Eq. (40). For the integration over \mathbf{r}' in Eq. (40) we adopt a similar scheme as for the functional itself. Due to the step functions in Eqs. (42)–(44) in region A the cutoff Δ can be replaced by the distance r for which the derivative is evaluated. In region B two terms from the lattice sum contribute. Because the integrand is nonanalytic at the lines where one of the distances d equals $\sigma/2 - r$, $\sigma/2$, or $\sigma/2 + r$ we partitioned the integration region B appropriately for the numerical integration. Together with the ideal free energy Eq. (10) one readily obtains the stationarity equation

$$\begin{aligned} \rho_\Delta(r) &= \frac{\exp\{-(1/4\pi r^2)[\delta \beta F_{\text{ex}}/N/\delta \rho_\Delta(r)]\}}{4\pi \int dr' r'^2 \exp\{-(1/4\pi r'^2)[\delta \beta F_{\text{ex}}/N/\delta \rho_\Delta(r')]\}}. \end{aligned} \quad (45)$$

Again a mesh is introduced for $\rho_\Delta(r)$ and the weighted densities are calculated by the trapezoidal rule with linear interpolation between the mesh points. More sophisticated numerical integration routines are used for the integration over \mathbf{r}' in Eq. (40) for regions A and B, and Eq. (45) is iterated until the maximum relative change in $\rho_\Delta(r)$ is less than 10^{-5} .

The resulting profiles for FMT1 are displayed in Fig. 7. They are almost constant at small r and then decrease steeper around $r = a/2$, increasingly fast upon approaching the close-packing limit. In the next section we show that the limiting shape indeed is a simple step function. The profiles for FMT2 shown in Fig. 8 exhibit a much smoother, Gaussian-like decay and their width, measured, e.g., by $\langle r^2 \rangle = \int d^3 r r^2 \rho_\Delta(r)$, on the scale a is considerably larger than for both the RY and FMT1 functionals. Clearly, again the absolute width goes to zero linearly with a , as expected in the close-packing limit.

C. Close-packing limit

As for the Ramakrishnan-Yussouff functional we assume that asymptotically the density profile has the form Eq. (14) with $\Delta = \sigma\delta$. We have seen that in the important range the

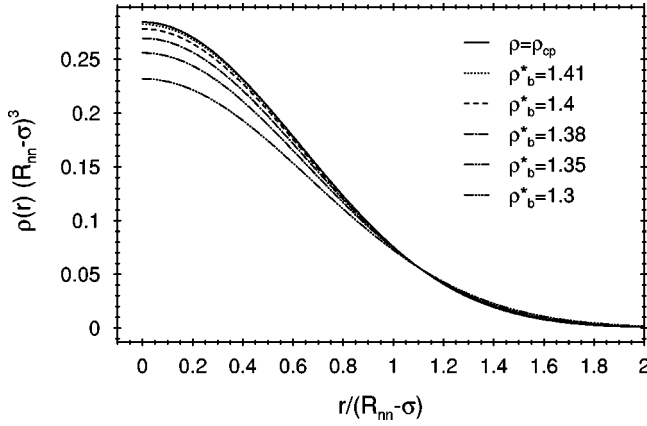


FIG. 8. Density profiles obtained from the improved fundamental-measure theory FMT2.

argument of the weighted densities is close to $\sigma/2$. Therefore we set $r/\sigma = 1/2 + t\delta$ and determine the leading contributions to $n_{\Delta}^{(\alpha)}(r)$ for small δ and fixed t :

$$n_{\Delta}^{(3)}(t) = \sum_{i=0}^{\infty} n_{3i}(t) \delta^i = 2\pi \left[2\Theta(-t) \int_0^{-t} ds s^2 \rho_0(s) + \int_{|t|}^{\infty} ds s \rho_0(s) [(s-t) + \delta(t^2 - s^2) + 2\delta^2 t(s^2 - t^2) + \dots] \right] \quad (46)$$

$$n_{\Delta}^{(2)}(t) = \frac{1}{\sigma} \sum_{i=0}^{\infty} n_{2i}(t) \delta^{i-1} = \frac{2\pi}{\sigma\delta} \int_{|t|}^{\infty} ds s \rho_0(s) (1 - 2t\delta + 4t^2\delta^2 + \dots) \quad (47)$$

$$\mathbf{n}_{\Delta}^{(V2)}(\hat{\mathbf{r}}, t) = \hat{\mathbf{r}} \frac{2\pi}{\sigma\delta} \int_{|t|}^{\infty} ds s \rho_0(s) \times [1 - 2t\delta + (6t^2 - 2s^2)\delta^2 + \dots], \quad (48)$$

$$n_{\Delta}^{(11)}(t) = 4\pi\delta \int_{|t|}^{\infty} ds s \rho_0(s) (s^2 - t^2 + \dots), \quad (49)$$

$$n_{\Delta}^{(33)}(t) = \frac{2\pi}{\delta} \int_{|t|}^{\infty} ds s \rho_0(s) [1 - 2t\delta + 4(2t^2 - s^2)\delta^2 + \dots], \quad (50)$$

where the caret denotes a unit vector. Since for any $\rho_0(s)$ the first two terms in the expansions of $n_{\Delta}^{(2)}$ and $|\mathbf{n}_{\Delta}^{(V2)}|$ are identical one has $n_2^2 - n_{V2}^2 = O(\delta^0)$ in region A. On the other hand, in region B the contributions to \mathbf{n}_{V2} from the two lattice sites have almost opposite directions so that $n_2^2 - n_{V2}^2 \sim \delta^{-2}$ there. For FMT2 we find $\det \hat{\mathbf{n}} \sim \delta$ in both regions, because, due to the quadratic dependence of $\mathbf{w}_{ij}(\mathbf{r})$ on the components of \mathbf{r} , the two contributions do not cancel each other in region B. Taking into account that the volumes of A and B are proportional to δ and δ^2 , respectively, we can estimate the order of the individual free energy contributions $\Phi_i = N^{-1} \int d^3r \phi_i[n_{\alpha}(\mathbf{r})]$:

	A	B
Φ_1	δ^0	δ
Φ_2	δ	δ^0
Φ_3^{FMT1}	δ^4	δ^{-1}
Φ_3^{FMT2}	δ^2	δ^3

Thus at this point a qualitative difference between the two approximations arises, as different terms become dominant in the close-packing limit. We first discuss FMT1, for which Φ_{3B} is the leading term. In a cylindrical coordinate system (z', ρ', ϕ') , centered at the midpoint between two sites and with its axis directed towards (see Fig. 6) one of them, the distances r_{\pm} to the sites, which occur as the argument of the weighted densities $n_{\Delta}^{(\alpha)}$, are

$$r_{\pm} = [\rho'^2 + (z' \pm R_{nn}/2)^2]^{1/2}. \quad (51)$$

In the scaled coordinates $\rho = \rho' / (\delta\sigma^2)$ and $z = z' / (\delta\sigma)$ one has $t_{\pm} = 1/2 + \rho \pm z + O(\delta)$ and

$$n_2^2 - n_{V2}^2 = \frac{4}{\delta^2} n_{20}(t_+) n_{20}(t_-) + \dots \quad (52)$$

which finally yields

$$\Phi_{3B}^{\text{FMT1}} \simeq \frac{32}{\delta} \int_0^{\infty} d\rho \int_0^{\infty} dz \left(\frac{n_{20}(t_+) n_{20}(t_-)}{n_{20}(t_+) + n_{20}(t_-)} \right)^3 \times \frac{1}{[1 - n_{30}(t_+) - n_{30}(t_-)]^2}. \quad (53)$$

Since $n_{30}(t) \in [0, 1]$ and $n_{20}(t) \geq 0$ this expression is positive. It attains its minimum value zero for all profiles $\rho_0(s)$ that have a strict cutoff at $s = 1/2$ so that region B is empty. In this restricted class of profiles the dominant contributions are Φ_{1A} and F_{id} . The former can be written as

$$\Phi_{1A} = - \int_{-1/2}^{1/2} dt n_{20}(t) \ln[1 - n_{30}(t)] + O(\delta). \quad (54)$$

But the fact that $n_{20}(t) = -\partial n_{30}/\partial t$ implies $\Phi_{1A} = 1 + O(\delta)$ for all profiles. Since here the peaks around different sites are independent of each other, this result is consistent with the extensively discussed 0D limit of the fundamental-measure functional [11,28]: For density profiles $\rho_{\Delta}(\mathbf{r})$ constrained to a volume that cannot hold more than one particle the exact excess free energy is $\beta F_{\text{ex}} = 1$ if $\int d^3r \rho_{\Delta}(\mathbf{r}) = 1$. One of the merits of the present theory is that this limit is almost exactly fulfilled [11]. At last we are left with the ideal free energy Eq. (15) as the only relevant $O(\delta^0)$ term, which, naturally, favors an evenly distributed density:

$$\rho_0(s) \rightarrow \frac{6}{\pi} \Theta\left(\frac{1}{2} - s\right). \quad (55)$$

This finding implies that the usually assumed Gaussian peaks represent a particularly bad approximation in this case. Indeed, in the Appendix we show that the width Δ of the best Gaussian is asymptotically related to the free distance a by $a \sim \Delta \sqrt{\ln(-\Delta)}$ which means that the ratio Δ/a tends to zero, albeit very slowly. The intuitive reason is that the tail of the

Gaussian profile leads to an unfavorable free energy contribution Φ_{3B} that can only be kept small if the tail increasingly “retracts.”

Actually the above arguments for the asymptotic step function shape in FMT1 can be generalized to nonspherical profiles. Starting from

$$\rho_{\Delta}(\mathbf{r}) = \frac{1}{\Delta^3} \rho_0(\mathbf{r}/\Delta) \quad (56)$$

and setting again $\mathbf{s} = \mathbf{r}/\Delta$, $\Delta = \sigma\delta = a$, and $|\mathbf{r}|/\sigma = 1/2 + t\delta$ one has

$$n_{\Delta}^{(3)}(\hat{\mathbf{r}}, t) = \int d^3s \Theta(\hat{\mathbf{r}}\mathbf{s} - t - \delta(t^2 - 2t\hat{\mathbf{r}}\mathbf{s} + s^2)) \rho_0(\mathbf{s}). \quad (57)$$

Expanding for small δ gives

$$n_{\Delta}^{(3)}(\hat{\mathbf{r}}, t) = \int d^3s \Theta(\hat{\mathbf{r}}\mathbf{s} - t) \rho_0(\mathbf{s}) + O(\delta). \quad (58)$$

Analogously we find

$$\begin{aligned} n_{\Delta}^{(2)}(\hat{\mathbf{r}}, t) &= \int d^3s \rho_0(\mathbf{s}) \\ &\times \left[\frac{1}{\delta} \delta(\hat{\mathbf{r}}\mathbf{s} - t) - (t^2 - 2t\hat{\mathbf{r}}\mathbf{s} + s^2) \delta'(\hat{\mathbf{r}}\mathbf{s} - t) + O(\delta) \right] \end{aligned} \quad (59)$$

and, using $\mathbf{n}_{\Delta}^{(V2)}(\mathbf{r}) = -\nabla n_{\Delta}^{(3)}(\mathbf{r})$,

$$\begin{aligned} n_{\Delta}^{(2)}(\hat{\mathbf{r}}, t) &= \int d^3s \rho_0(\mathbf{s}) \\ &\times \left[\frac{1}{\delta} \hat{\mathbf{r}} \delta(\hat{\mathbf{r}}\mathbf{s} - t) - \hat{\mathbf{r}}(t^2 - 2t\hat{\mathbf{r}}\mathbf{s} + s^2) \right. \\ &\left. \times \delta'(\hat{\mathbf{r}}\mathbf{s} - t) - 2[\mathbf{s} - (\hat{\mathbf{r}}\mathbf{s})\hat{\mathbf{r}}] \delta(\hat{\mathbf{r}}\mathbf{s} - t) + O(\delta) \right]. \end{aligned} \quad (60)$$

Since the last term in this equation is perpendicular to $\hat{\mathbf{r}}$ the combination $n_2^2 - n_{V2}^2$ is still of order δ^0 in region A. If in region B the same coordinates (z, ρ, ϕ') as before are used and the vectors to the nearest lattice sites are denoted by \mathbf{r}_{\pm} , the fact that $\hat{\mathbf{r}}_+ \hat{\mathbf{r}}_- = -1 + O(\delta)$ yields $n_2^2 - n_{V2}^2 = O(\delta^{-2})$. Thus, in summary all estimates for the individual terms given in the table above remain valid. Again the dominant term Φ_{3B} is positive and minimized by cutoff profiles. As the leading terms of the scalar weighted densities are related by $n_{20}(\hat{\mathbf{r}}, t) = -\partial n_{30}(\hat{\mathbf{r}}, t)/\partial t$ the contribution Φ_{1A} in leading order is still independent of the profile. The ideal term now enforces $\rho_{\Delta}(\mathbf{r})$ to be constant in the maximum allowed region C that is compatible with $B = \emptyset$. It can be constructed by shifting the bounding planes of the Wigner-Seitz cell inward by $\sigma/2$ (see Fig. 9). A given point \mathbf{r} in C contributes to the weighted densities at \mathbf{r}' only if $|\mathbf{r} - \mathbf{r}'| \leq \sigma/2$. By construction all such \mathbf{r}' lie within the Wigner-Seitz cell and thus cannot be “reached” from any \mathbf{r} in the cell C' around another site, which means that B is indeed empty. However if a point P outside of C were added the distance to its mirror

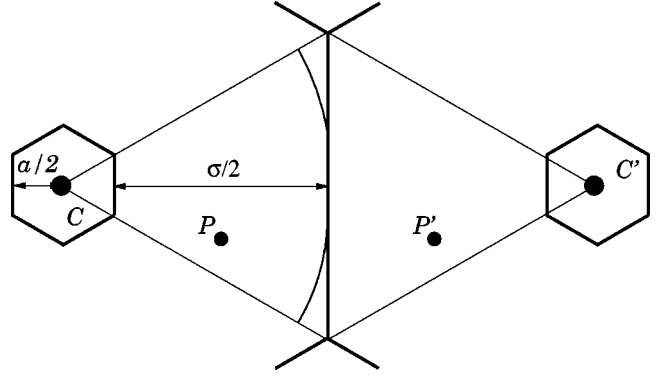


FIG. 9. Illustration of the cells C for which the fundamental measure theory predicts a constant density (a 2D analogon of the 3D crystal is drawn). The circular arcs and their straight connection limit the set of points whose distance to C is smaller than $\sigma/2$, i.e., the region A. The point P cannot belong to C because otherwise P' would belong to C' and some points in between would have distances smaller than $\sigma/2$ from both C and C', i.e., region B would be nonempty.

point P' with respect to the closest Wigner-Seitz boundary plane would be less than σ so that elements of B would lie on their joining line (see Fig. 9). The cell C constructed here is identical to that of the self-consistent cell theory [23]. Its volume for an fcc solid is $a^3/\sqrt{2}$.

We now turn to the second approximation (FMT2) for which Φ_{2B} and F_{id} are the dominant contributions. [Remember that Φ_{1A} is independent of $\rho_0(s)$ in leading order.] Analogous to Eq. (53) we have, neglecting higher orders in δ ,

$$\Phi_{2B} \approx 24 \int_0^\infty d\rho \int_0^\infty dz \frac{n_{20}(t_+) n_{20}(t_-)}{1 - n_{30}(t_+) - n_{30}(t_-)} \quad (61)$$

with $t_{\pm} = 1/2 + \rho \pm z$. The corresponding stationarity equation is

$$\rho_0(s) = \frac{\exp\{-(1/4\pi s^2)[\delta\Phi_{2B}/\delta\rho_0(s)]\}}{4\pi \int_0^\infty ds' s' \exp\{-(1/4\pi s'^2)[\delta\Phi_{2B}/\delta\rho_0(s')]\}}. \quad (62)$$

The functional derivative is calculated as in Sec. III B. The resulting asymptotic profile shown in Fig. 8 is close to those obtained for finite densities using the full functional. It is almost, but not exactly Gaussian.

The asymptotic free energy of the fundamental-measure theory also has the form Eq. (22). In FMT1 one has $f_0 = \frac{1}{2} \ln 2 = 0.3466$. Under the constraint of spherical symmetry this is replaced by $f_0 = \ln(6/\pi) = 0.6470$, both of which are much closer to the correct value than the Ramakrishnan-Yussouff theory. Results for finite distance from close packing are given in Fig. 5 and agree, probably by accident, rather well with the computer simulations. The approach to the asymptotic law is quite slow. On the other hand for FMT2 not only the profiles but also the free energies (Fig. 5) approach their asymptotic limit faster in this version of the theory. The value of the constant in Eq. (22) is found to be $f_0 = -1.527$ in very good agreement with the MD results. However, in view of the relatively large change in f_0 due to

nonsphericity of the profiles as observed for FMT1, this may well be fortuitous. We did not consider nonspherical profiles in FMT2.

D. Saddle point

In view of the discussion in the introduction it would be interesting also to keep track of the saddle point between the liquid and the solid state when close packing is approached. Unfortunately, again one is plagued by the fact that the iteration of the stationarity equation does not converge to a second solution. Furthermore the arguments of the asymptotic analysis do not apply to the saddle point because they essentially involve a minimization in two steps. Hence one must revert to parametrizations of the density with a few parameters. For Gaussians and step functions the saddle point occurs at a width Δ proportional to $a^{2/3}$ in FMT1 and to $a^{1/2}$ in FMT2. However, a priori there is no reason to assume that at the saddle point the profile has a similar shape as at the minimum. We also tried profiles of the forms $\rho_{\Delta}(r) \sim \exp[-(r/\Delta)^n]$ and $\rho_{\Delta}(r) \sim (1+r/\Delta)^{-n}$ and found numerically that in both cases the free energy at the maximum with respect to Δ decreases with decreasing n , down to the lowest feasible values of n . This suggests that the actual saddle point profile may decay very slowly, while within these restricted classes of profiles a true saddle point at a nondegenerate profile seems not to exist.

IV. MONTE CARLO SIMULATIONS

Although an extensive computer simulation study of the density distribution in hard-sphere crystals has been carried out before [14], no useful results for the radial distribution function have been published. In order to assess the quality of the various theories we therefore undertook a small Monte Carlo (MC) simulation ourselves. In an NVT ensemble of 8^3 spheres in an fcc arrangement we measured the distribution of the particles' distance r from their equilibrium sites. We corrected for the movement of these sites due to shifts in the center of mass. Measurements were taken over 2×10^6 MC steps per particle for two bulk densities. The results are plotted in Fig. 10 on a logarithmic scale versus $(r/a)^2$ and compared to the various DFT calculations. The quantitative agreement is excellent for FMT2. The profiles are close to Gaussians but decay faster at large distance than a Gaussian fitted to the small distance part. The dependence of the scaled profiles on bulk density is rather small in the examined range, but still qualitatively reproduced by the theory. The actual width of the profiles will increase with increasing particle number [14], but we did not attempt to correct for finite size effects. In Ref. [14] it was found that in the thermodynamic limit for high densities the width behaves as $\langle r^2 \rangle^{1/2}/a = 1.098 \pm 0.004$, again in almost perfect agreement with FMT2, for which $\langle r^2 \rangle^{1/2}/a = 1.025$. This means that FMT2 is the first DFT which yields the correct value of the Lindemann parameter.

V. SUMMARY AND DISCUSSION

In summary, we have analyzed the close-packing limit of the hard-sphere crystal using three versions of DFT. All of them predict a peak width Δ that vanishes proportional to the free distance a and yields a logarithmic term in the free en-

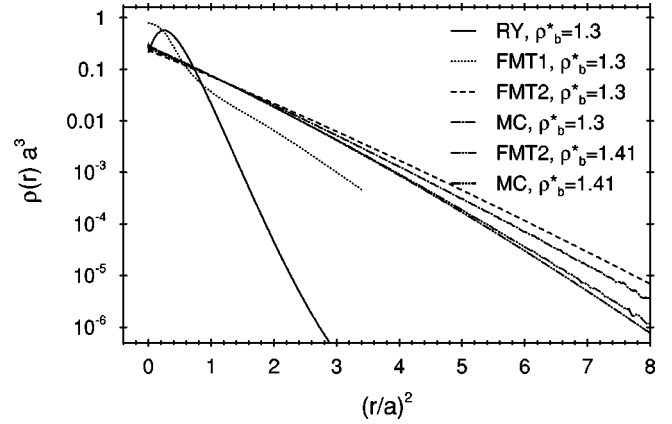


FIG. 10. Comparison of the density profiles from Monte-Carlo simulation and the density-functional theory FMT2 for two bulk densities. A Gaussian profile would correspond to a straight line in this plot.

ergy [see Eq. (22)] stemming from the ideal gas entropy. Numerically this has been observed before, for Gaussian peaks, in two other DFTs, the generalized liquid approximation (GELA) and the modified weighted density approximation (MWDA) [29]. For the latter, however, it was found later that the solutions correspond to ‘‘unphysical’’ branches [30]. Results for the profile width $\langle r^2 \rangle^{1/2}$ obtained from all mentioned DFT versions are compared in Fig. 11. FMT2 and MWDA agree satisfactorily with the simulations, while the peak widths predicted by GELA is considerably smaller but still larger than those of FMT1 and RY. The relative performance of the different theories can also be judged from the profile shape obtained by free minimization. RY gives too narrow profiles with an unphysical maximum if the bulk density is used as the expansion point (Fig. 2). The shape and width are also wrong for other expansion points (Fig. 3). FMT1 predicts asymptotically steplike profiles confined to the cells of cell theory (Fig. 7). Only the FMT2 profiles (Fig. 8) are in quantitative agreement with simulations at high densities (Fig. 10). In spite of the anharmonicity of the hard-sphere crystal they are close to Gaussians. The GELA and

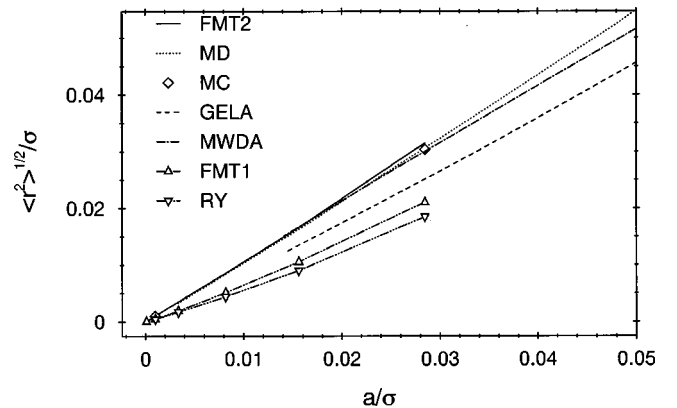


FIG. 11. The peak widths $\langle r^2 \rangle^{1/2}$ near the close packing density obtained from different versions of DFT and computer simulations. The GELA and MWDA data were taken from Ref. [29] and the molecular dynamics (MD) results for 500 particles from Ref. [14]. The diamonds denote our Monte Carlo simulations with 512 particles.

MWDA results were obtained under the assumption of Gaussian peaks. At present it is not clear what happens within these approximations if more general shapes are allowed nor whether the proportionality $\langle r^2 \rangle^{1/2} \sim a$ is strictly valid in the close-packing limit. The results for the next-to-leading free energy contribution also improve from RY to FMT1 to FMT2 (Fig. 5), the two FMT versions being much closer to the correct result than RY. This could have been expected from the way the RY approximation is constructed: A density expansion around a liquid state certainly is difficult to justify for the highly ordered high-density crystal.

If one restricts the profiles to a fixed shape saddle points of the free energy are found at widths decaying $\sim a^x$ with $x_{\text{RY}}=1$, $x_{\text{FMT1}}=2/3$, and $x_{\text{FMT2}}=1/2$. Insofar the global scenario for the crystalline solutions proposed in the introduction is confirmed (see also Fig. 4). However, as detailed in Sec. III D, in larger classes of functions the saddle point remains elusive. We remark that the saddle point is a property closely connected to the mean-field type free energy functional and, e.g., is not directly accessible by computer simulations.

Comparing the two variants of FMT we see that the structure in the close-packing limit is sensitive to subtle differences between DFT approximations and thus might be a guiding line in the construction of better FMT-like functionals. Besides our FMT1 some other approximations for ϕ_3 have been suggested in Ref. [11] which are all of the form

$$\phi_3 = \frac{n_2^3}{(1-n_3)^2} f(\xi) \quad \text{with} \quad \xi = |\xi| = \left| \frac{\mathbf{n}_{V2}}{n_2} \right|. \quad (63)$$

The power of n_2 is determined by dimensional arguments and the function f can only depend on the absolute value of ξ because of the isotropy of space. From Eqs. (47) and (48) we have $\xi = 1 + O(\delta^2)$ in region A. In order not to spoil the correct leading order for a quasi-zero-dimensional situation as given by Φ_{1A} one has the additional requirement $f(\xi \rightarrow 1) \sim (1-\xi)^n$ with $n \geq 2$, which implies $\Phi_{3A} \sim \delta^{2n-2}$. But in region B ξ varies between zero and one so that always $\Phi_{3B} \sim \delta^{-1}$. The function f must be nonnegative in this range, otherwise the functional would not be bounded from below [this happened in the original FMT [10] for which $f(\xi) = (1/3 - \xi^2)/(8\pi)$]. Then the argument of Sec. III C runs through and the asymptotic profiles will always be step functions. We conclude that an improved description of the high density solid is not possible within FMT if only the scalar and vector weighted densities are used, the tensor weight function of FMT2 is inevitable. On the other hand in FMT2 the behavior near close packing is exclusively determined by ϕ_2 so that no conditions on the precise form of ϕ_3 can be deduced.

Note added in proof. Very recently we learned of an improved FMT version derived by Tarazona [31] which replaces Eq. (30) with

$$\Phi_3^{\text{FMT2}} = \frac{3}{16\pi} [\mathbf{n}_{V2} \cdot \hat{\mathbf{n}} \cdot \mathbf{n}_{V2} - n_2 \mathbf{n}_{V2}^2 - \text{tr}(\hat{\mathbf{n}}^3) + n_2 \text{tr}(\hat{\mathbf{n}}^2)].$$

Using the methods of the present work, we could show that this modification does not alter the profile shape in the close-packing limit or the value of f_0 .

ACKNOWLEDGMENTS

We thank Sander Pronk for providing the Monte Carlo program and Y. Rosenfeld for stimulating discussions. This work is part of the research program of the Stichting voor Fundamenteel Onderzoek der Materie (Foundation for Fundamental Research on Matter) and was made possible by financial support from the Nederlandse Organisatie voor Wetenschappelijk Onderzoek (Netherlands Organization for the Advancement of Research). B.G. acknowledges the financial support of the EU.

APPENDIX: GAUSSIAN PEAKS IN FMT1

For Gaussian density peaks $\rho_0(s) = \pi^{-3/2} e^{-s^2}$ the leading contributions to the weighted densities are [see Eqs. (46)–(48)]

$$n_{30}(t) = \frac{1}{2} [1 - \text{erf}(t)], \quad n_{20}(t) = \frac{1}{\sqrt{\pi}} e^{-t^2} \quad (A1)$$

and for a width $\Delta = a/(2\alpha)$ the dominant excess free energy contribution is [see Eq. (53)]

$$\begin{aligned} \Phi_{3B} &= \frac{32}{\pi^{3/2}} \frac{\sigma}{\Delta} \int_0^\infty d\rho \int_0^\infty dz [e^{(\rho+\alpha+z)^2} + e^{(\rho+\alpha-z)^2}]^{-3} \\ &\times \left[\frac{1}{2} \text{erf}(\rho + \alpha + z) + \frac{1}{2} \text{erf}(\rho + \alpha - z) \right]^{-2} + O(\Delta^0). \end{aligned} \quad (A2)$$

In order that F_{ex} does not become too large for $a \rightarrow 0$ we expect $\alpha \rightarrow \infty$. In this limit the substitutions $\rho' = \rho\alpha$ and $z' = z\alpha$ yield

$$\Phi_{3B} = \frac{1}{12\sqrt{\pi}} \frac{\sigma}{\Delta} \frac{\exp(-3\alpha^2)}{\alpha^2}. \quad (A3)$$

Now we can add

$$\beta F_{id}/N = -\frac{3}{2} \ln \pi (\Delta/\lambda)^2 - \frac{5}{2} \quad (A4)$$

and minimize with respect to Δ which gives

$$\frac{\sigma}{\Delta} \frac{1}{2\sqrt{\pi}} \exp\left(-\frac{3}{4} \frac{a^2}{\Delta^2}\right) = 3. \quad (A5)$$

This equation indeed has a solution with $\Delta/a \rightarrow 0$ for $a \rightarrow 0$; solved for a one has

$$a = \frac{2\Delta}{\sqrt{3}} \left[-\ln \left(6\sqrt{\pi} \frac{\Delta}{\sigma} \right) \right]^{1/2} \quad (A6)$$

which demonstrates that Δ/a decays only very slowly. Nevertheless this decay is at variance with the physical expectation $\Delta/a \rightarrow \text{const}$ which is well supported by computer simulations [14] and, as shown in the main text, is also fulfilled within the present theory if allowance is made for more general profile shapes.

- [1] S. Alexander and J. McTague, *Phys. Rev. Lett.* **41**, 702 (1978).
- [2] B. Groh and B. Mulder, *Phys. Rev. E* **59**, 5613 (1999).
- [3] Y. Singh, *Phys. Rep.* **207**, 351 (1991).
- [4] R. Evans, in *Fundamentals of Inhomogeneous Fluids*, edited by D. Henderson (Marcel Dekker, New York, 1992), Chap. 3, pp. 85–175.
- [5] A. Haymet, in *Fundamentals of Inhomogeneous Fluids*, edited by D. Henderson (Marcel Dekker, New York, 1992), Chap. 9, pp. 363–405.
- [6] R. Ohnesorge, Ph.D. thesis, Universität München, 1994.
- [7] N. Ashcroft, in *Density Functional Theory*, edited by E. Gross and R. Dreizler (Plenum, New York, 1995), pp. 581–623.
- [8] T. Ramakrishnan and M. Yussouff, *Phys. Rev. B* **19**, 2775 (1979).
- [9] A. Haymet, *J. Chem. Phys.* **78**, 4641 (1983).
- [10] Y. Rosenfeld, *Phys. Rev. Lett.* **63**, 980 (1989).
- [11] Y. Rosenfeld, M. Schmidt, H. Löwen, and P. Tarazona, *Phys. Rev. E* **55**, 4245 (1997).
- [12] R. Ohnesorge, H. Löwen, and H. Wagner, *Europhys. Lett.* **22**, 245 (1993).
- [13] B. Laird, J. McCoy, and A. Haymet, *J. Chem. Phys.* **87**, 5449 (1987).
- [14] D. Young and B. Alder, *J. Chem. Phys.* **60**, 1254 (1974).
- [15] J. P. Hansen and I. McDonald, *Theory of Simple Liquids*, 2nd ed. (Academic, London, 1986).
- [16] M. Baus and J. Colot, *Mol. Phys.* **55**, 653 (1985).
- [17] M. Baus, *J. Phys.: Condens. Matter* **1**, 3131 (1989).
- [18] Y. Rosenfeld, *J. Phys.: Condens. Matter* **8**, L795 (1996).
- [19] Y. Rosenfeld and P. Tarazona, *Mol. Phys.* **95**, 141 (1998).
- [20] R. Kayser and H. Raveché, *Phys. Rev. A* **17**, 2067 (1978).
- [21] J. Scheurle, *J. Math. Anal. Appl.* **59**, 596 (1977).
- [22] R. Buehler, R. Wentorf, J. Hirschfelder, and C. Curtiss, *J. Chem. Phys.* **19**, 61 (1950).
- [23] J. Kirkwood, *J. Chem. Phys.* **18**, 380 (1950).
- [24] W. Wood, *J. Chem. Phys.* **20**, 1334 (1952).
- [25] W. Hoover, *J. Chem. Phys.* **43**, 371 (1965).
- [26] Z. Salsburg and W. Wood, *J. Chem. Phys.* **37**, 798 (1962).
- [27] B. Alder, W. Hoover, and D. Young, *J. Chem. Phys.* **49**, 3688 (1968).
- [28] P. Tarazona and Y. Rosenfeld, *Phys. Rev. E* **55**, R4873 (1997).
- [29] C. Tejero, M. Ripoll, and A. Pérez, *Phys. Rev. E* **52**, 3632 (1995).
- [30] C. Tejero, *Phys. Rev. E* **55**, 3720 (1997).
- [31] P. Tarazona, *Phys. Rev. Lett.* **84**, 694 (2000).